Journal of *Marine Science and Engineering*

MDPI

*Article*

# Topographical Mitigation of Surge Flows: A Lagrangian Study on the Shielding Effect of Erodible Marine Beds

**Kyung Sung Kim**

Department of Mechatronics Convergence Engineering, Changwon National University, Changwon 51140, Republic of Korea; keiuskim@changwon.ac.kr; Tel.: +82-55-213-3846

**Abstract**

Dam-break flows over erodible beds represent a complex fluid–solid interaction problem characterized by extreme turbulence and rapid morphological changes. This study investigates the dynamics of such flows over inclined granular beds by integrating an advanced Moving Particle Semi-implicit (MPS) method. To accurately resolve the transition between static and kinetic granular regimes, I introduce a state-dependent tangential friction model that explicitly distinguishes between sticking and sliding conditions based on local force balance. Furthermore, the momentum exchange between the fluid and solid phases is rigorously modeled using the porosity-dependent drag formulation. The numerical results demonstrate a distinct regime shift in energy dissipation: while low-inclination beds (0–4%) promote distributed sediment transport, steep-inclination beds (8–12%) trigger a localized "Shielding Effect". In this regime, the surge's horizontal kinetic energy is rapidly converted into vertical potential energy and frictional work, forming a deep sacrificial scour hole that acts as a topographical energy sink. This mechanism effectively mitigates the destructive potential of the surge in downstream areas. The proposed method provides a robust tool for predicting morphological feedback and designing topographical countermeasures for disaster mitigation in hydraulic and coastal environments.

**Keywords:** moving particle semi-implicit method; computational fluid dynamics; solid–fluid interaction

## 1. Introduction

Dam-break flows represent one of the most extreme transient hydraulic phenomena, characterized by the sudden release of stored potential energy and the rapid formation of highly nonlinear free-surface waves. Such flows exhibit intense turbulence, strong momentum exchange, and large deformation of the free surface, often resulting in severe flooding, structural damage, and substantial seabed deformation. Understanding and predicting the dynamics of dam-break flows therefore remain a critical issue in hydraulic, coastal, and geotechnical engineering.

The fundamental behavior of dam-break waves has been widely studied using analytical, experimental, and numerical approaches. Early analytical investigations employed the method of characteristics to describe wave propagation and front evolution under idealized conditions [1]. Recent numerical studies have focused on the interaction between water flow and coastal protection structures, emphasizing the importance of accurate turbulence modeling and validation against experimental data to predict inundation patterns [2]. Experimental studies demonstrated that dam-break flows are often accompanied

Check for updates

Academic Editors: Marcello Di Risio and Piera Fischione

Received: 3 March 2026
Revised: 27 March 2026
Accepted: 1 April 2026
Published: 2 April 2026

**Copyright:** © 2026 by the authors. Licensee MDPI, Basel, Switzerland. This article is an open access article distributed under the terms and conditions of the Creative Commons Attribution (CC BY) license.

by strong turbulence and significant energy dissipation mechanisms, including turbulent drag reduction [3].

Beyond purely hydrodynamic aspects, the interaction between dam-break flows and movable beds has received increasing attention. One-dimensional and depth-averaged models have been proposed to describe dam-break flows over erodible beds, highlighting the coupling between flow momentum and bed evolution [4]. More advanced numerical studies examined sediment transport and morphodynamics induced by dam-break swash uprushes, emphasizing the importance of coupled fluid–sediment modeling strategies [5]. The role of strong turbulence and complex free-surface boundary conditions in such high-energy environments was further clarified by Brocchini and Peregrine [6,7].

Conventional grid-based computational fluid dynamics (CFD) methods have been widely used to simulate free-surface and multiphase flows. Hybrid particle–mesh techniques have also been developed to combine the strengths of Eulerian and Lagrangian methods [8,9]. However, these mesh-based or hybrid methods often suffer from numerical diffusion, reduced accuracy in tracking highly distorted interfaces, and difficulties in handling large deformation and fragmentation of the free surface, particularly in dam-break scenarios involving violent impact and sediment motion [10,11].

Fully Lagrangian particle-based methods provide an effective alternative for simulating such complex flows without artificial interface smoothing. Among them, Smoothed Particle Hydrodynamics (SPH), originally introduced by Monaghan [12], has been extensively applied to free-surface and fluid–solid interaction problems. Comprehensive reviews have summarized recent advances in SPH methodology, including improvements in numerical consistency, stability, and convergence [13,14]. SPH-based models have also been successfully applied to problems involving solid body transport in urban flash floods [15,16], as well as to mobile-bed dam-break problems [17,18].

Another representative particle-based approach is the Moving Particle Semi-Implicit (MPS) method, originally proposed by Koshizuka and co-workers [19,20]. The MPS method solves the incompressible Navier–Stokes equations using a particle interaction model and a pressure Poisson equation, enabling stable and accurate simulation of violent free-surface motion and fluid fragmentation [21–23]. Subsequent improvements addressed pressure stabilization and smoothing issues, further enhancing numerical robustness [24,25]. Comparative studies demonstrated that the MPS method can provide sharper free-surface resolution and more stable pressure fields than standard weakly compressible SPH formulations [26].

The MPS method has also been extended to specialized fluid–solid and fluid–structure interaction problems. For example, Kim et al. [27] developed an MPS-based approach for multiliquid-layer sloshing, while Kim [28] applied a mesh-free particle method to simulate mobile-bed behavior induced by dam-break flows. More recently, improved particle methods have been proposed to enhance the accuracy of fluid–structure interaction simulations [29].

The mechanical behavior of granular beds is governed by contact, collision, and frictional interactions. The Discrete Element Method (DEM) provides a fundamental model for modeling granular assemblies [30]. Experimental and theoretical investigations have shown that frictional state transitions and granular dilatancy play a crucial role in controlling bed mobility and energy dissipation in dam-break-induced sheet flows [31]. In recent work, Kim (2021) [32] proposed a new particle interaction model for solid particles, which was later extended by Kim (2025) [33] to analyze sediment transport dynamics under violent free-surface flows.

Building upon these previous studies, the present work introduces a state-dependent friction model within the MPS method. Unlike unified friction models, this extended for-

mulation explicitly distinguishes between static and kinetic friction regimes based on local contact conditions and force balance. This enables a more physically consistent representation of the initiation of motion and energy dissipation. The proposed model is applied to investigate the "Shielding Effect" of inclined erodible beds, providing mechanistic insights into how topographical reconfiguration can localize the destructive potential of surge flows and protect downstream environments.

## 2. Methodology

### *2.1. Moving Particle Semi-Implicit Method*

#### 2.1.1. Fluid Particle Method

The Moving Particle Semi-Implicit (MPS) method, originally proposed by Koshizuka and Oka [20], is a fully Lagrangian particle-based numerical approach developed for the simulation of incompressible free-surface flows. In the MPS method, the fluid domain is represented by discrete particles that move according to local interactions, enabling a natural treatment of large free-surface deformation and fragmentation without explicit interface tracking.

The governing equations for fluid particle motion consist of the incompressibility condition and the Navier–Stokes equation, expressed as follows:

$$\frac{D\rho}{Dt} = 0 \tag{1}$$

$$\frac{D\vec{u}}{Dt} = -\frac{1}{\rho}\nabla P + \nu\nabla^2\vec{u} + \vec{g} \tag{2}$$

Here, $\rho$ denotes the particle density, $\vec{u}$ is the particle velocity, $\nu$ is the kinematic viscosity, and $\vec{g}$ represents gravitational acceleration. The pressure gradient term enforces incompressibility, while the viscous term models momentum diffusion within the fluid.

In the MPS method, spatial derivatives appearing in the governing equations are approximated using particle interaction models. The gradient, divergence, and Laplacian operators are evaluated through weighted summations over neighboring particles:

$$\langle\nabla\phi\rangle_i = \frac{d}{n_0}\sum_{j\neq i}\left[\frac{\phi_{ij}\vec{r}_{ij}}{|\vec{r}_{ij}|^2}\,w(|\vec{r}_{ij}|)\right] \tag{3}$$

$$\langle\nabla\cdot\phi\rangle_i = \frac{d}{n_0}\sum_{j\neq i}\left[\frac{\phi_{ij}\cdot\vec{r}_{ij}}{|\vec{r}_{ij}|^2}\,w(|\vec{r}_{ij}|)\right] \tag{4}$$

$$\langle\nabla^2\phi\rangle_i = \frac{2d}{\lambda n_0}\sum_{j\neq i}\left[\phi_{ij}\,w(|\vec{r}_{ij}|)\right], \qquad \lambda = \frac{\sum_{j\neq i}\left[|\vec{r}_{ij}|^2 w(|\vec{r}_{ij}|)\right]}{\sum_{j\neq i}\left[w(|\vec{r}_{ij}|)\right]} \tag{5}$$

where $\phi$ denotes an arbitrary physical quantity, $d$ is the number of spatial dimensions, and $n_0$ is the reference particle number density. The kernel function $w(|\vec{r}_{ij}|)$ defines the influence range of neighboring particles within the effective interaction radius $r_e$:

$$w(|\vec{r}_{ij}|) = \begin{cases} \left(1-\dfrac{|\vec{r}_{ij}|}{r_e}\right)^3\left(1+\dfrac{|\vec{r}_{ij}|}{r_e}\right)^3, & 0 \le |\vec{r}_{ij}| < r_e, \\ 0, & |\vec{r}_{ij}| \ge r_e. \end{cases} \tag{6}$$

In this study, the value of $r_e$ is carefully selected based on the initial particle spacing to ensure sufficient neighbor support for numerical stability, following standard practices in the MPS method.

2.1.2. Solid Particle Method

In dense granular media, such as movable seabeds, mechanical behavior is governed primarily by inter-particle contact, friction, and force chain formation rather than viscous diffusion. To address this, I reformulate the MPS method for solid particles by replacing the viscous stress term with a contact-based friction model. The governing equation for solid particle motion is expressed as:

$$\rho_s \frac{D\vec{u}_s}{Dt} = -\nabla P + \vec{F}_f + \vec{F}_{drag} + \vec{g} \tag{7}$$

where $\rho_s$ is the solid particle density, $\vec{u}_s$ is the velocity of the solid phase, $\vec{F}_f$ represents the frictional force arising from inter-particle contact, and $\vec{F}_{drag}$ denotes the drag force exerted by the fluid.

In this study, the momentum exchange between the fluid and solid phases is modeled by incorporating the drag force $\vec{F}_{drag}$. To accurately represent the interaction in both dense and dilute regimes, I adopt the drag model proposed by Wen (1966) [34]. The drag force is evaluated as:

$$\vec{F}_{drag} = \frac{\beta}{\rho_s}(\vec{u}_f - \vec{u}_s) \tag{8}$$

where $\vec{u}_f$ is the local fluid velocity and $\beta$ is the momentum exchange coefficient. In accordance with the fluidization mechanics proposed by Wen [34], the coefficient $\beta$ is formulated to account for the porosity-dependent drag enhancement:

$$\beta = \frac{3}{4} C_D \frac{(1-\alpha_f)\alpha_f \rho_f |\vec{u}_f - \vec{u}_s|}{d_p} \alpha_f^{-2.65} \tag{9}$$

Here, $\alpha_f$ represents the local fluid volume fraction (porosity), $d_p$ is the particle diameter, $\rho_f$ is the fluid density, and $C_D$ is the standard drag coefficient. The term $\alpha_f^{-2.65}$ serves as a correction factor for the increased drag in multiparticle systems, which is essential for resolving the "Shielding Effect" as it governs the interfacial momentum dissipation over the erodible bed.

The frictional interaction $\vec{F}_f$ is activated only under compressive normal contact. The normal-force-based contribution $\vec{F}_f^{(1)}$ is evaluated as:

$$\begin{gathered} \vec{F}_f^{(1)} = \sum_{j \neq i} \frac{1}{2}(\mu_i + \mu_j)\left(\rho_j \vec{a}_{n,j} - \rho_i \vec{a}_{n,i}\right)\vec{t}_{ij}, \\ \text{where } \left(\rho_j \vec{a}_{n,j} - \rho_i \vec{a}_{n,i}\right) > 0, \text{ otherwise } \vec{F}_f^{(1)} = 0. \end{gathered} \tag{10}$$

To resolve the transition between static and kinetic regimes, a state-dependent tangential friction model is employed. The sticking condition is enforced when:

$$\left|\mathbf{F}_t^{\text{drive}}\right| \leq \mu_s |\mathbf{F}_n| \implies \mathbf{F}_t = -\mathbf{F}_t^{\text{drive}} \tag{11}$$

Once the threshold is exceeded, the kinetic friction regime is applied:

$$\mathbf{F}_t = -\mu_k |\mathbf{F}_n| \frac{\mathbf{u}_t}{|\mathbf{u}_t|} \tag{12}$$

This formulation provides a physically consistent representation of motion initiation and energy dissipation under transient surge flows. A schematic illustration of the state-dependent friction model and neighbor particle interactions is shown in Figure 1.

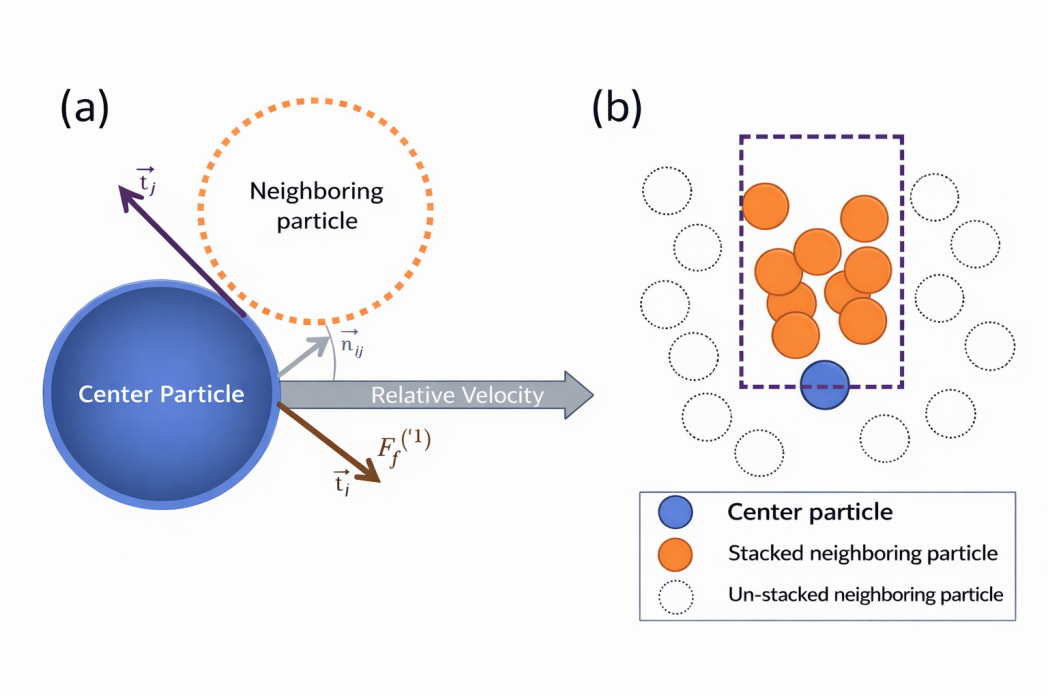



**Figure 1.** Schematic (**a**) Interaction between a center particle and a neighboring particle showing the relative velocity direction, normal unit vector, and resulting friction force. (**b**) Conceptual arrangement of stacked and un-stacked neighboring particles around the center particle.

In the present formulation, the tangential friction behavior is modeled using a state-dependent framework that explicitly distinguishes between sticking and sliding regimes. Unlike conventional DEM-based Coulomb friction models, where tangential forces are typically evaluated as continuous functions of relative velocity, the present approach introduces a force-balance-based switching criterion.

Specifically, the transition between static and kinetic friction is determined by comparing the driving tangential force with the static friction threshold. When the driving force remains below the threshold, particles remain in a sticking state, ensuring that no artificial slip occurs. Once the threshold is exceeded, the model transitions to the kinetic regime, where the tangential force is limited by the kinetic friction coefficient.

This formulation enables a more physically consistent representation of motion initiation and energy dissipation under highly transient flow conditions, particularly in scenarios involving rapid force fluctuations such as dam-break-induced sediment transport. In contrast to previous formulations, the present model explicitly resolves the regime transition at each time step, allowing improved prediction of localized energy dissipation and scour initiation.

### *2.2. Non-Dimensional Framework and Governing Parameters*

To enhance the generality of this study and facilitate comparison with other hydraulic and sediment transport research, I introduce a non-dimensional framework. The dynamic behavior of the surge flow and its interaction with the erodible bed are governed by three primary dimensionless parameters.

First, the Froude number ($Fr$) represents the ratio of inertial to gravitational forces:

$$Fr = \frac{U}{\sqrt{gH}} \tag{13}$$

where $U$ is the characteristic velocity and $H$ is the fluid depth. In the present dam-break configurations, the flow is inertia-dominated ($Fr > 1$), indicating strong free-surface deformation and rapid surge propagation upon impact with the inclined bed.

Second, for sediment transport dynamics, the Shields number ($\theta$) is employed to characterize the ratio of bed shear stress to the submerged weight of the particles:

$$\theta = \frac{\tau}{(\rho_s - \rho) g d_p} \tag{14}$$

where $\tau$ is the bed shear stress and $d_p$ is the particle diameter. This parameter determines the onset of particle motion and governs the transition between stable and mobile bed conditions. In this study, the high Shields number at the slope toe facilitates the transition to an active transport state.

Third, the relative submergence ($H/d_p$) indicates the scale separation between the fluid depth and the particle size. In the present simulations, $H/d_p \gg 1$, ensuring that bulk flow structures and near-bed interactions are both adequately resolved within the MPS method.

Importantly, the proposed state-dependent friction model introduces additional dimensionless control through the friction coefficients ($\mu_s$, $\mu_k$). These regulate the transition between sticking and sliding regimes, providing a mechanism to capture energy dissipation that is not solely governed by hydrodynamic shear but also by granular contact dynamics.

The emergence of the "Shielding Effect" can be interpreted within this framework as a regime shift driven by the interplay between $Fr$, $\theta$, and the bed slope. As the inclination increases, the system transitions from a transport-dominant regime (distributed shear) to an impact-dominant regime characterized by localized high stress and rapid energy dissipation. This non-dimensional interpretation demonstrates that the observed behavior reflects a general physical mechanism governing surge–bed interaction rather than a specific geometric artifact.

## 3. Numerical Simulation Results

### 3.1. Flat Mobile Bed Problem and Validation

This section presents the numerical results obtained using the proposed MPS-based fluid–solid interaction model. To ensure the reliability of the simulation, the model is first validated against the experimental data reported by Spinewine [31].

Figure 2 illustrates the initial setup for validation. The domain captures the fundamental transition of potential energy into kinetic energy upon gate release. The high-resolution particle spacing ($1.0 \times 10^{-4}$ m) is critical for resolving the thin shear layer at the fluid–solid interface, where steep velocity gradients govern the initiation of sediment transport.

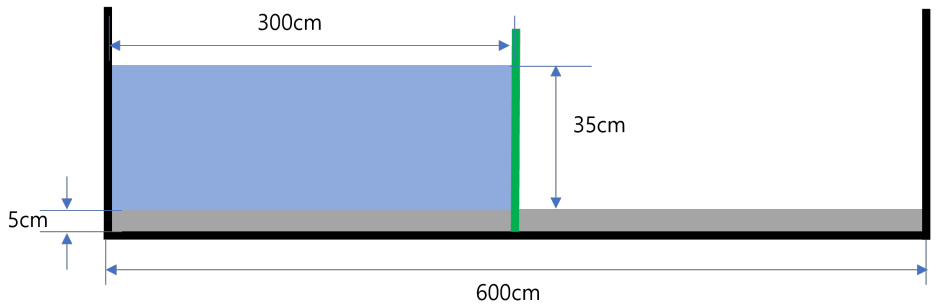



**Figure 2.** Computational setup for the dam-break simulation over a mobile sediment bed.

As shown in Figure 3, the MPS simulation successfully replicates the collapse of the water column and the subsequent bed deformation. The morphological evolution, characterized by the formation of initial and secondary dune structures, demonstrates

that the MPS method effectively resolves the momentum exchange from the fluid phase to the granular phase. The close agreement in the surge front's arrival time confirms that the proposed interaction model accurately captures the threshold of motion for granular particles under high-shear transient flows.

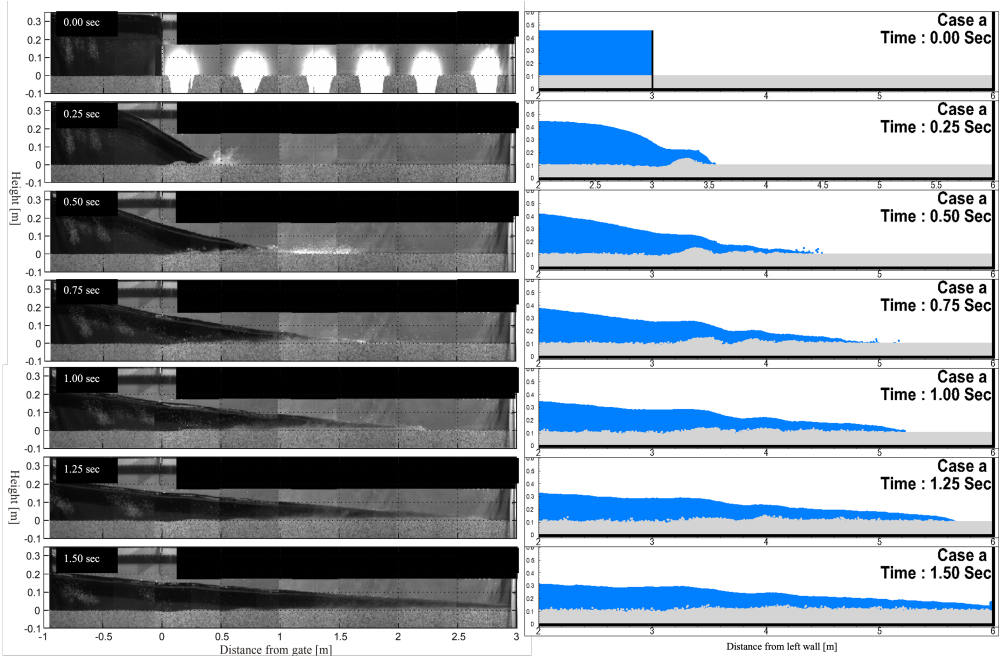



**Figure 3.** Comparison between experimental observations and MPS simulation results for validation.

To investigate the mitigation effect of sediment mobility, Figure 4 compares the mobile-bed with a fixed-bed configuration. In the fixed-bed case, the wave front reaches the downstream wall before $t = 1.0$ s due to the lack of boundary resistance. In contrast, the mobile-bed case exhibits a significant delay (reaching the wall at $t \approx 1.5$ s). This delay is a direct consequence of energy partition; a substantial portion of the surge's kinetic energy is consumed to overcome the inertia of sediment particles and inter-particle friction. This observation validates the "buffering capacity" of erodible beds, where the bed acts as a sacrificial topographical energy sink.

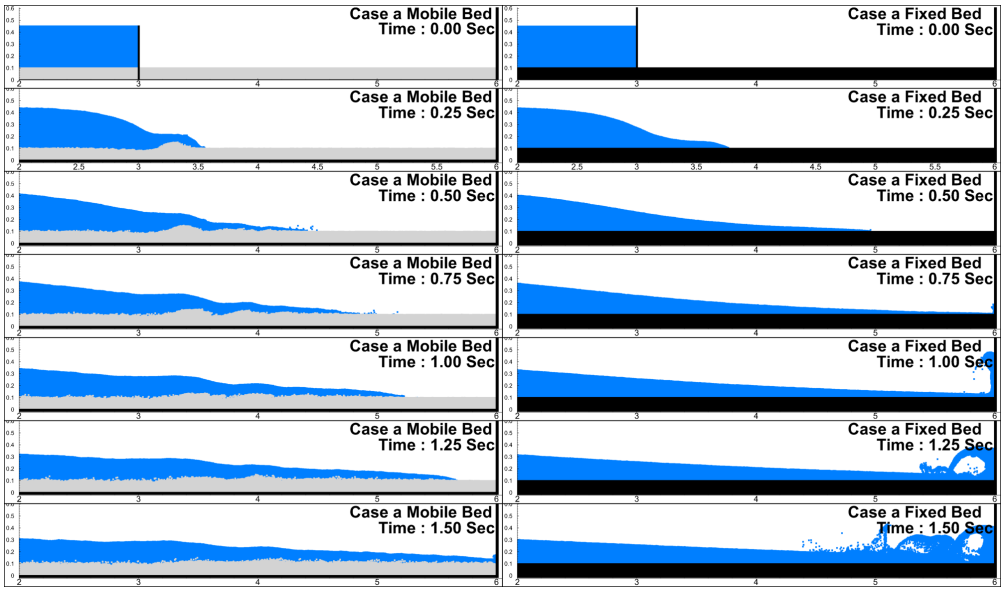



**Figure 4.** Comparison of flow evolution between fixed-bed and mobile-bed cases.

Quantitative Validation

To further substantiate the agreement, the time evolution of the surge front position is compared with experimental data.

The root-mean-square error (RMSE) is defined as:

$$RMSE = \sqrt{\frac{1}{N}\sum_{i=1}^{N}(x_{sim,i} - x_{exp,i})^2} \quad (15)$$

The computed RMSE indicates good quantitative agreement between the simulation and experimental observations.

To provide a rigorous quantitative assessment of the proposed mobile bed model, the sediment height profiles were compared by aligning the computational domain with the experimental setup of Spinewine [31] and sampling at $N = 100$ uniformly distributed $x$-coordinates. The numerical results accurately capture the experimental sediment morphology, including the characteristic formation and equilibrium slope of the sand dune.

Following the validation approach commonly used in high-fidelity surge flow studies (e.g., [2]), this agreement is substantiated by a low Root Mean Square Error (RMSE) of 0.0045 m at $t = 0.5$ s, which effectively validates the accuracy and predictive capability of the present MPS-based solver. A more comprehensive discussion regarding the grid convergence, parameter sensitivity, and detailed validation metrics for this specific numerical framework is provided in my previous work by Kim (2025) [33].

### *3.2. Effect of Bed Inclination (0%, 4%, 8%, 12%)*

Following validation, the influence of bed topography was examined using four slope configurations.

Figure 5 presents the geometric variations used to analyze topographical effects. The rise in bed elevation (0.12 m to 0.36 m) directly influences the potential energy barrier. From a fluid dynamics perspective, the slope introduces a vertical momentum component, forcing a reconfiguration of the flow's energy structure upon impact.

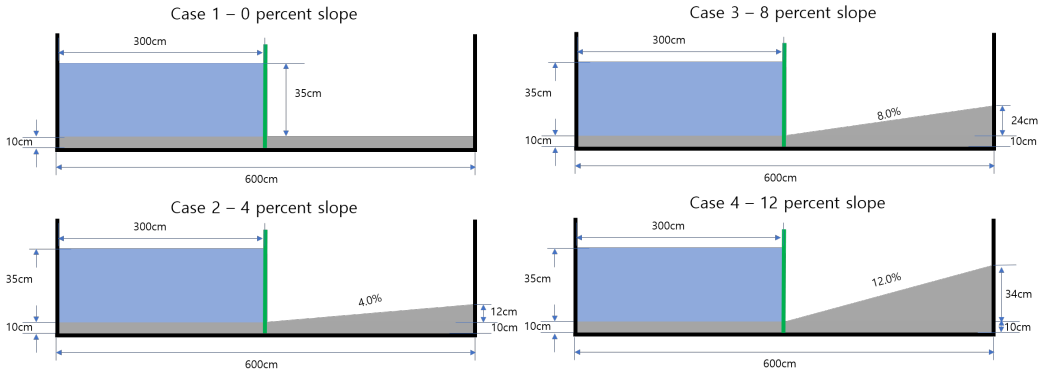
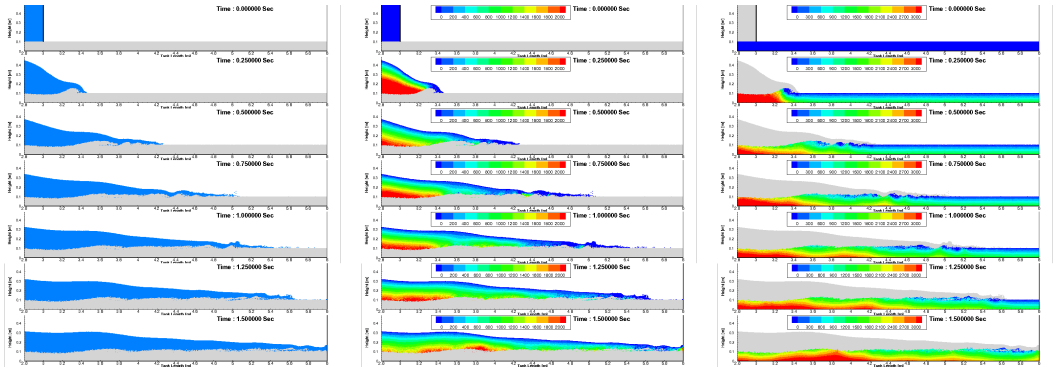



**Figure 5.** Simulation Model of dam-break flow over various slopes.

#### 3.2.1. Detailed Analysis of the 0% Slope (Flat Bed)

For the 0% slope (Figure 6), the flow is characterized by horizontal propagation. The fluid pressure (b) follows a quasi-hydrostatic distribution, suggesting that vertical accelerations are negligible. The solid pressure (c) remains relatively low and uniform, indicating that sediment transport is driven primarily by surface shear stress (traction) rather than concentrated normal impact.

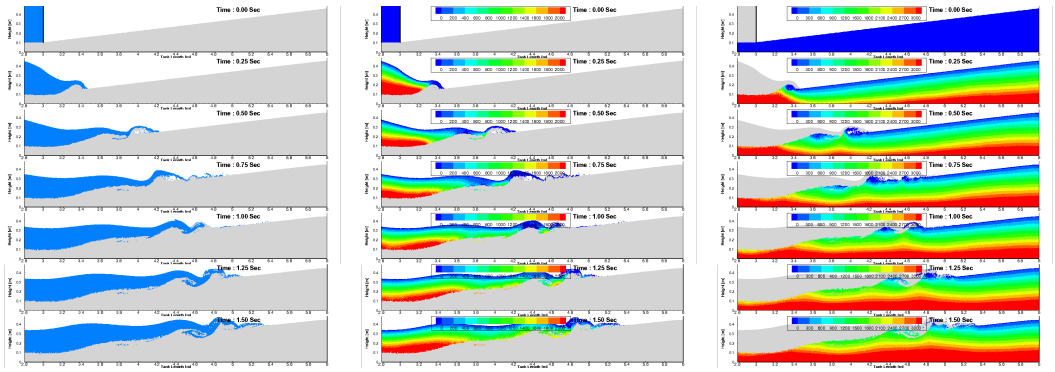


(a) (b) (c)

**Figure 6.** Time-series snapshots (from $t = 0.0$ to 1.5 s) comparing (**a**) particle positions, (**b**) fluid pressure, and (**c**) solid pressure for the 0% slope case. The quasi-hydrostatic pressure distribution indicates a transport-dominant regime where flow momentum is preserved horizontally.

#### 3.2.2. Detailed Analysis of the 12% Slope (Impact-Dominant Regime)

The 12% slope (Figure 7) exhibits extreme energy localization. The vertical splashing in (a) indicates that horizontal kinetic energy is being diverted vertically upon impact. The fluid pressure field (b) reveals a high-intensity stagnation zone at the slope toe, acting as a hydraulic jump that induces localized turbulence. This impact generates a concentrated solid pressure peak (c), which is the primary driver for the rapid formation of a deep scour hole.



(a) (b) (c)

**Figure 7.** Time-series snapshots (from $t = 0.0$ to 1.5 s) comparing (**a**) particle positions, (**b**) fluid pressure, and (**c**) solid pressure for the 12% slope case. The quasi-hydrostatic pressure distribution indicates a transport-dominant regime where flow momentum is preserved horizontally.

#### 3.2.3. Comparative Analysis at $t = 0.50$ s

At $t = 0.50$ s (Figure 8), the kinematic divergence between the slope configurations becomes prominent. In the 12% slope case, the surge exhibits a pronounced vertical "run-up" behavior, whereas the 0% case maintains a purely horizontal propagation. This vertical diversion serves as the primary mechanism for converting the surge's horizontal kinetic energy into potential energy, effectively arresting the front velocity.

The fluid pressure distribution in Figure 9 corroborates this energy conversion. A high-intensity stagnation zone forms at the toe of the 12% slope, where the fluid velocity is abruptly reduced. This pressure localization indicates that the surge's destructive energy is being consumed instantaneously upon impact, rather than being transported further downstream.

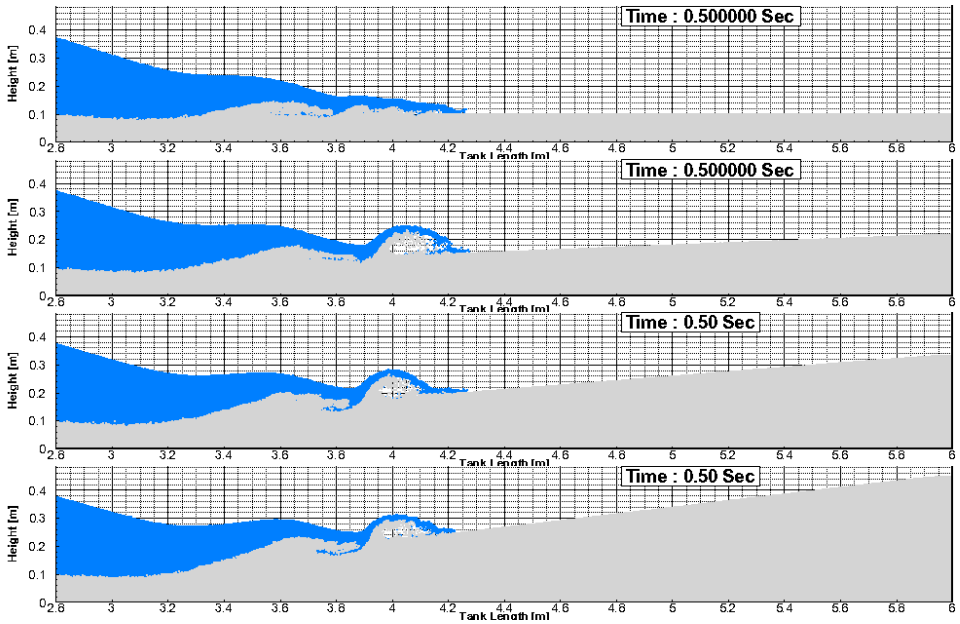



**Figure 8.** Comparison of particle positions for 0%, 4%, 8%, and 12% slope cases at $t = 0.50$ s. As the inclination increases, the flow regime shifts from horizontal translation to vertical energy dissipation at the toe.

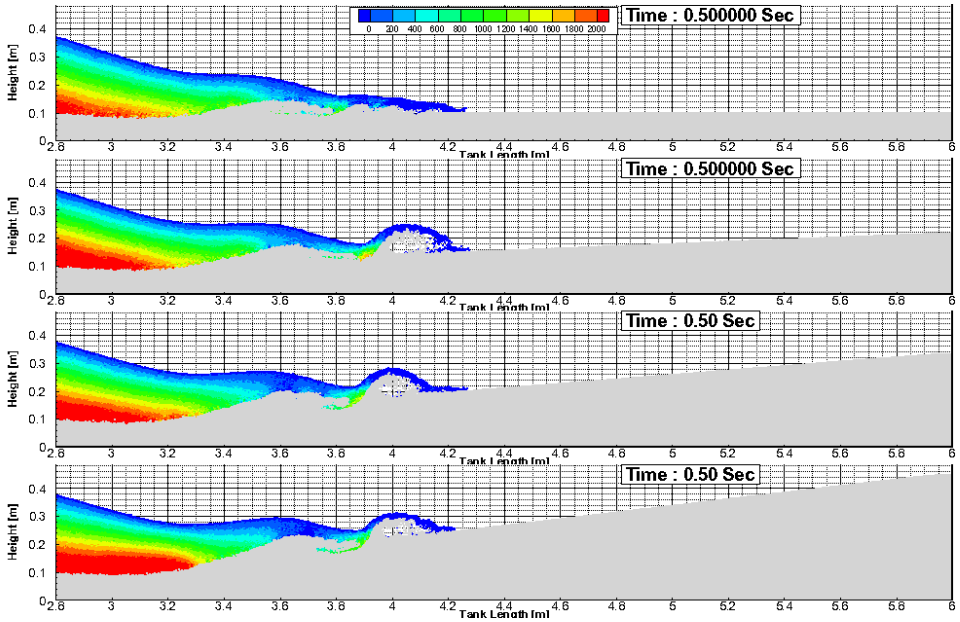



**Figure 9.** Fluid pressure distribution for 0%, 4%, 8%, and 12% slope cases at $t = 0.50$ s. A high-intensity stagnation zone forms at the toe of the 12% slope, indicating localized energy dissipation that triggers the Shielding Effect.

The solid pressure in Figure 10 shows that the bed stress is most concentrated in the 12% case. This localized stress exceeds the threshold of motion for the granular particles, facilitating the immediate initiation of a deep scour hole at the point of impact.

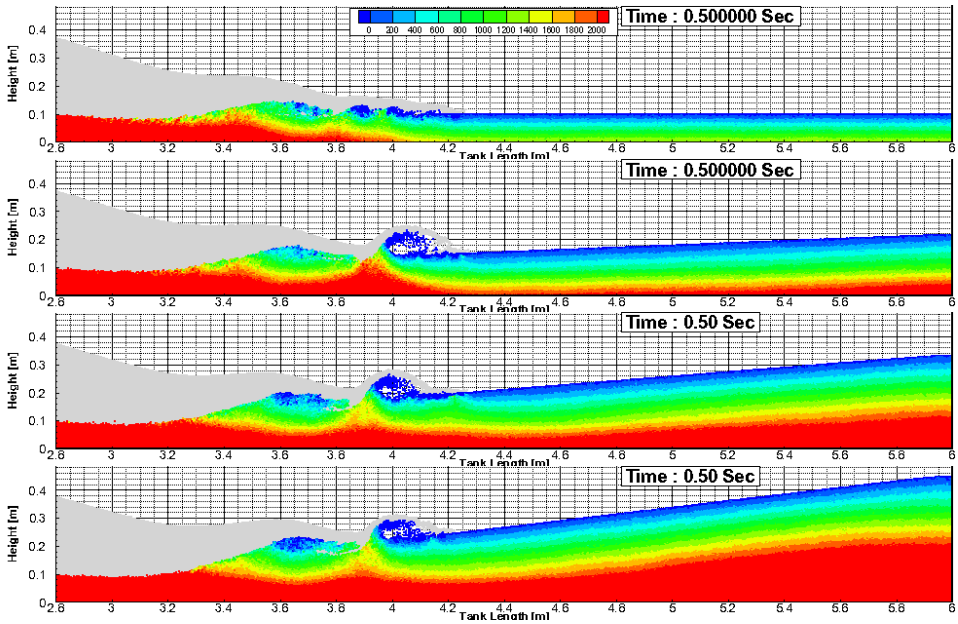



**Figure 10.** Solid pressure distribution for 0%, 4%, 8%, and 12% slope cases at $t = 0.50$ s. The concentrated pressure peak at the 12% slope toe demonstrates how topographical steepness focuses impact forces to initiate the scouring process.

### 3.2.4. Temporal Evolution at $t = 0.75$ s and $t = 1.00$ s

By $t = 0.75$ s (Figure 11), the 12% slope case reaches a stabilized localized impact regime. The wave front is effectively captured at the upstream face of the incline. In contrast, the 4% slope case allows significant residual energy to propagate past the toe, indicating that gentle slopes are insufficient to fully dissipate the surge's momentum.

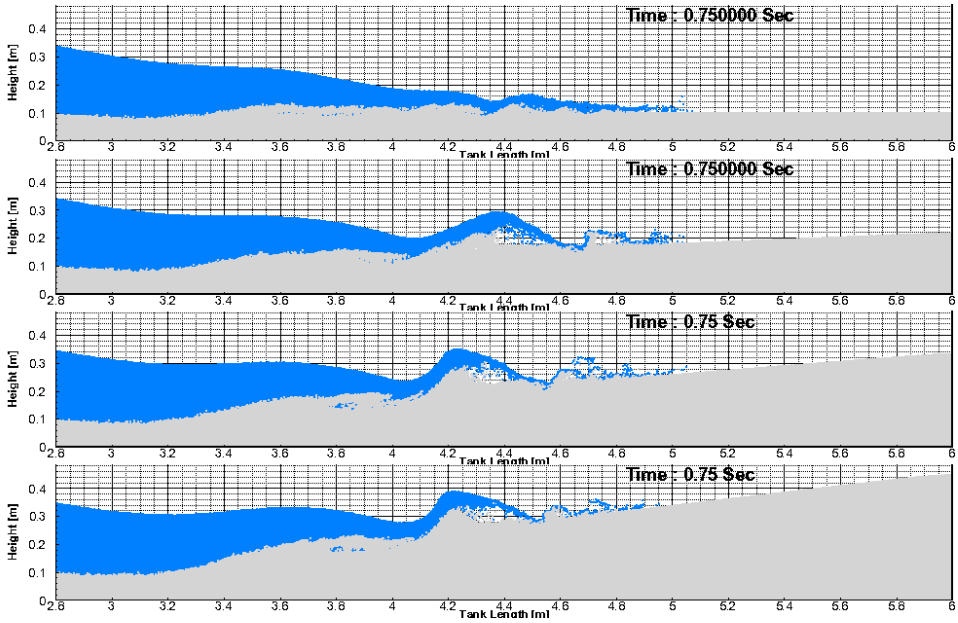



**Figure 11.** Comparison of bed profiles for 0%, 4%, 8%, and 12% slope cases at $t = 0.75$ s. The 12% case shows a clearly defined quiescent zone downstream, protected by the upstream topographical energy sink.

At $t = 1.00$ s (Figure 12), the "Shielding Effect" reaches full maturity. For the 12% slope, the downstream region remains undisturbed by high-velocity flows, as the surge energy is trapped within the sacrificial scour hole. Conversely, the 0% and 4% cases exhibit

widespread scouring and wave propagation that extends toward the far boundary of the domain.

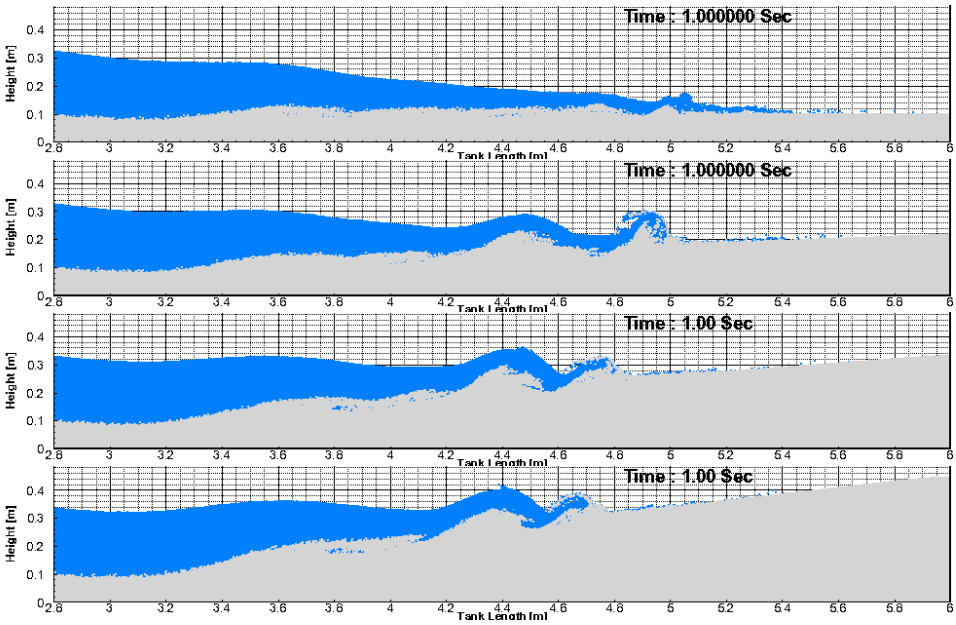



**Figure 12.** Comparison of bed profiles for 0%, 4%, 8%, and 12% slope cases at $t = 1.00$ s. The depth of the sacrificial scour hole increases with slope steepness, effectively anchoring the surge's destructive potential.

The fluid pressure at $t = 1.00$ s (Figure 13) confirms that for steep slopes, the high-pressure zone remains anchored at the toe. This persistent energy sink prevents the downstream transmission of high-pressure surges, validating the deterministic role of topography in flood mitigation.

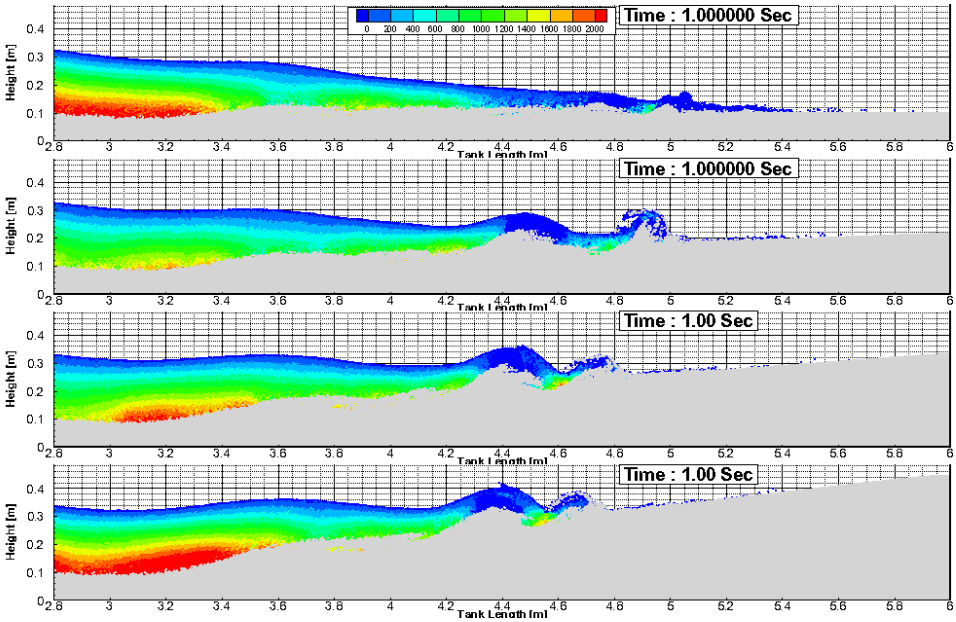



**Figure 13.** Fluid pressure distribution for 0%, 4%, 8%, and 12% slope cases at $t = 1.00$ s. The persistence of the high-pressure zone at the slope toe for steep cases confirms the continuous damping of surge intensity.

Finally, the solid pressure in Figure 14 illustrates the exhaustion of scouring potential in the 12% case. The stress downstream converges to near-zero values, confirming that steep

topographical features can confine the hydro-morphological impact within a predefined buffer zone, thereby protecting the broader downstream ecosystem.

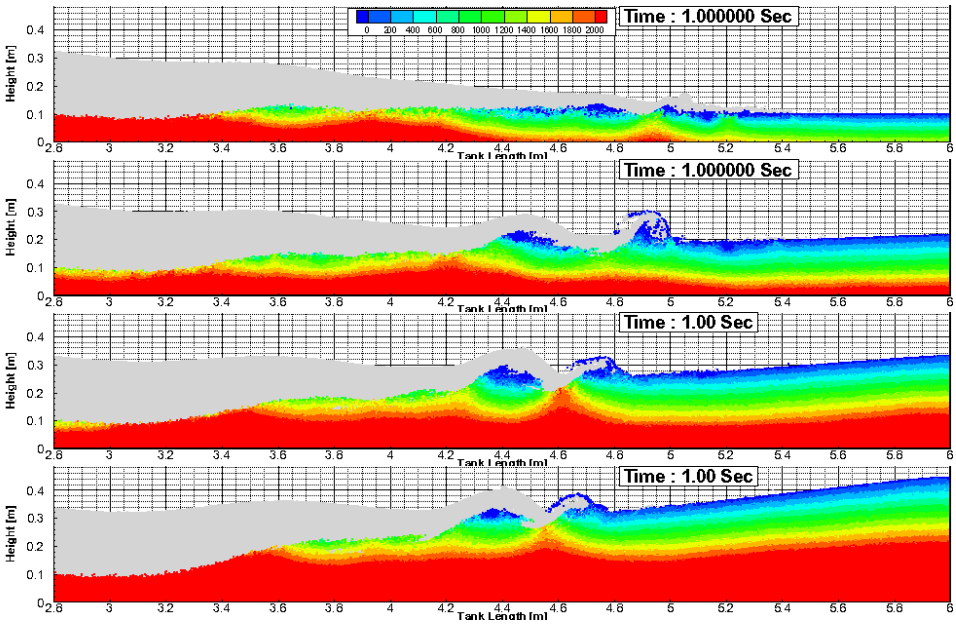



**Figure 14.** Solid pressure distribution for 0%, 4%, 8%, and 12% slope cases at $t = 1.00$ s. The near-zero stress in the downstream region for the 12% slope case proves that steep features can confine the hydro-morphological impact.

3.2.5. Mechanistic Synthesis: Regime Transition and Shielding Efficacy

A comparative synthesis of the results reveals a fundamental shift in the energy dissipation mechanism as a function of bed inclination. The interaction can be categorized into two distinct physical regimes:

- Transport-dominant Regime (0–4%): In these cases, energy is dissipated through distributed surface friction over an extended domain. The surge maintains a high momentum flux, resulting in widespread downstream erosion. The bed mobility acts as a "moving conveyor," transporting sediment rather than arresting the wave front.
- Impact-dominant Regime (8–12%): As the inclination increases, the slope acts as a deterministic barrier. The horizontal kinetic energy is instantaneously converted into vertical potential energy and stagnation pressure. The resulting scour hole creates a self-reinforcing energy trap; as the sacrificial scour hole deepens, it enhances fluid entrapment and significantly reduces the energy available for downstream propagation.

Ultimately, these results demonstrate that steep topographical features do not merely resist flow but actively reconfigure the surge's energy structure, protecting the broader downstream ecosystem through the "Shielding Effect."

To further quantify the shielding effect beyond the qualitative description above, a dimensionless shielding efficiency is introduced based on the attenuation of flow energy across the erodible bed region.

Specifically, the shielding efficiency is defined as the relative reduction of depth-averaged kinetic energy between the upstream surge front and the downstream region after interaction with the bed deformation. This metric reflects the combined influence of bed-induced flow deceleration, momentum redistribution, and energy dissipation associated with sediment transport and scour formation.

In the present simulations, the shielding efficiency is evaluated for different slope conditions, allowing systematic comparison of the topographical mitigation performance.

The results indicate that the shielding effect is maximized within a specific slope range, where the formation of a localized scour hole enhances energy dissipation while preventing excessive flow acceleration.

This definition provides a consistent and physically interpretable criterion to distinguish between shielding-dominant and transport-dominant regimes.

### 3.3. Engineering Implications

The results indicate that bed inclination acts as a critical design parameter for surge mitigation. For slopes exceeding 8%, a transition to the impact-dominant regime occurs, leading to the formation of a sacrificial scour hole. This feature serves as a localized energy sink, trapping high-velocity fluid and protecting downstream infrastructure. I suggest that strategically engineered erodible topographies can be utilized as effective "soft" coastal protection measures.

## 4. Conclusions

In this study, a Lagrangian numerical method based on the Moving Particle Semi-implicit (MPS) method was developed to elucidate the complex fluid–solid coupling mechanisms during dam-break flows over erodible inclined beds. By integrating a state-dependent friction model into the MPS method, the proposed model successfully resolved the nonlinear transition between static and kinetic granular regimes, providing a robust tool for analyzing transient scouring processes. The primary scientific contributions and findings of this research are synthesized as follows:

First, the high-fidelity validation against experimental benchmarks confirms that the proposed MPS method accurately captures the morphological evolution of mobile sediment beds. A critical observation is that bed mobility itself functions as a natural energy buffer; the surge's potential energy is partially partitioned into sediment mobilization and inter-particle frictional work, resulting in a significant delay in wave propagation compared to fixed-bed configurations.

Second, the investigation into topographical effects identified a deterministic regime shift governed by bed inclination. For gentle slopes (0–4%), the system operates in a Transport-dominant Regime where energy dissipation is distributed longitudinally via skin friction, facilitating widespread sediment transport into the downstream domain. Conversely, steeper inclinations (8–12%) trigger an Impact-dominant Regime. In this regime, the surge's horizontal kinetic energy is instantaneously converted into vertical potential energy and localized stagnation pressure at the slope toe, radically reconfiguring the flow's momentum structure.

Third, this study establishes the concept of a "Shielding Effect" rooted in topographical feedback. This discovery suggests that topographical steepness can be a key design parameter for coastal protection structures. The steep inclination forces the formation of a localized, deep scour hole that serves as an effective energy sink. This morphological trap captures high-velocity fluid particles, thereby creating a downstream "quiescent zone" characterized by negligible bed stress and flow intensity. These findings suggest that strategically engineered erodible topographies can be utilized to localize the destructive potential of surge flows, providing a predictable buffer zone to protect vulnerable downstream infrastructure and ecosystems.

In conclusion, the present research offers both a robust numerical methodology and profound physical insights into the deterministic role of topography in coastal and riverine disaster mitigation. Future extensions of this work will incorporate three-dimensional complex terrains and multi-phase interactions involving heterogeneous, non-

uniform sediment distributions to further enhance the model's predictive capabilities in real-world scenarios.

**Funding:** This research received no external funding.

**Data Availability Statement:** The data presented in this study are available on request from the corresponding author.

**Conflicts of Interest:** The author declares no conflict of interest.

## References


1. Chanson, H. Application of the method of characteristics to the dam break wave problem. *J. Hydraul. Res.* **2009**, 47, 41–49. [CrossRef]
2. Iqbal, S.; Dissanayaka, K.D.C.R.; Tanaka, N. Numerical modeling and validation of dike-induced water flow dynamics using OpenFOAM. *ISH J. Hydraul. Eng.* **2024**, *30*, 559–573. [CrossRef]
3. Janosi, I.M.; Jan, D.; Szabo, K.G.; Tel, T. Turbulent drag reduction in dam break flows. *Exp. Fluids* **2004**, *37*, 219–220. [CrossRef]
4. Wu, W.M.; Wang, S.S.Y. One-dimensional modeling of dam break flow over movable beds. *J. Hydraul. Eng.* **2007**, *133*, 48–58. [CrossRef]
5. Postacchini, M.; Othman, I.K.; Brocchini, M.; Baldock, T.E. Sediment transport and morphodynamics generated by a dam-break swash uprush: Coupled vs. uncoupled modelling. *Coast. Eng.* **2014**, *89*, 99–105. [CrossRef]
6. Brocchini, M.; Peregrine, D.H. The dynamics of strong turbulence at free surfaces. Part 1. Description. *J. Fluid Mech.* **2001**, *449*, 225–254. [CrossRef]
7. Brocchini, M.; Peregrine, D.H. The dynamics of strong turbulence at free surfaces. Part 2. Free-surface boundary conditions. *J. Fluid Mech.* **2001**, *449*, 255–290. [CrossRef]
8. Ramaswamy, R.; Bourantas, G.; Jülicher, F.; Sbalzarini, I.F. A hybrid particle-mesh method for incompressible active polar viscous gels. *J. Comput. Phys.* **2015**, *291*, 334–361. [CrossRef]
9. Zhang, S.; Zhang, B.; Liu, X.; Shan, J. Application of a particle-grid hybrid method in multiphase flow calculation. *J. Nucl. Sci. Technol.* **2020**, *57*, 1199–1214. [CrossRef]
10. Juez, C.; Murillo, J.; Garcia-Navarro, P. A 2D weakly-coupled and efficient numerical model for transient shallow flow and movable bed. *Adv. Water Resour.* **2014**, *71*, 93–109. [CrossRef]
11. Juez, C.; Ferrer-Boix, C.; Murillo, J.; Hassan, M.A.; Garcia-Navarro, P. A model based on Hirano-Exner equations for two-dimensional transient flows over heterogeneous erodible beds. *Adv. Water Resour.* **2016**, *87*, 1–18. [CrossRef]
12. Monaghan, J.J. Simulating free surface flows with SPH. *J. Comput. Phys.* **1994**, *110*, 399–406. [CrossRef]
13. Lind, S.J.; Rogers, B.D.; Stansby, P.K. Review of smoothed particle hydrodynamics: Towards converged Lagrangian flow modelling. *Proc. R. Soc. A* **2020**, *476*, 20190801. [CrossRef] [PubMed]
14. Zhang, C.; Zhu, Y.J.; Wu, D.; Adams, N.A.; Hu, X. Smoothed particle hydrodynamics: Methodology development and recent achievement. *J. Hydrodyn.* **2022**, *34*, 767–805. [CrossRef]
15. Amicarelli, A.; Albano, R.; Mirauda, D.; Agate, G.; Sole, A.; Guandalini, R. A smoothed particle hydrodynamics model 3D solid body transport in free surface flows. *Comput. Fluids* **2015**, *116*, 205–228. [CrossRef]
16. Albano, R.; Sole, A.; Mirauda, D.; Adamowski, J. Modelling large floating bodies in urban area flash-floods via a smoothed particle hydrodynamics model. *J. Hydrol.* **2016**, *541*, 344–358. [CrossRef]
17. Shakibaeinia, A.; Jin, Y.C. A mesh-free particle model for simulation of mobile-bed dam break. *Adv. Water Resour.* **2011**, *34*, 794–807. [CrossRef]
18. Bui, H.H.; Nguyen, G.D. Smoothed particle hydrodynamics (SPH) and its applications in geomechanics: From solid fracture to granular behaviour and multiphase flows in porous media. *Comput. Geotech.* **2021**, *138*, 104315. [CrossRef]
19. Koshizuka, S.; Tamako, H.; Oka, Y. A Particle Method for Incompressible Viscous Flow with Fluid Fragmentation. *J. Comput. Fluid Dyn.* **1995**, *4*, 29–46.
20. Koshizuka, S.; Oka, Y. Moving-particle semi-implicit method for fragmentation of incompressible fluid. *Nucl. Sci. Eng.* **1996**, *123*, 421–434. [CrossRef]
21. Koshizuka, S.; Nobe, A.; Oka, Y. Numerical analysis of breaking waves using the moving particle semi-implicit method. *Int. J. Numer. Methods Fluids* **1998**, *26*, 751–760. [CrossRef]
22. Nomura, K.; Koshizuka, S.; Oka, Y.; Obata, H. Numerical analysis of drop breakup behavior using particle method. *J. Nucl. Sci. Technol.* **2001**, *38*, 1057–1064. [CrossRef]
23. Shirakawa, N.; Horie, H.; Yamamoto, Y.; Tsunoyama, S. Analysis of the void distribution in a circular tube with the two-fluid particle interaction method. *J. Nucl. Sci. Technol.* **2001**, *38*, 392–402. [CrossRef]

24. Lee, B.H.; Park, J.C.; Kim, M.H.; Hwang, S.C. Step-by-step improvement of MPS method in simulating violent free-surface motions and impact-loads. *Comput. Methods Appl. Mech. Eng.* **2011**, *200*, 1113–1125. [CrossRef]
25. Tanaka, M.; Masunaga, T. Stabilization and smoothing of pressure in MPS method by quasi-compressibility. *J. Comput. Phys.* **2010**, *229*, 4279–4290. [CrossRef]
26. Farid, P.B.; Kim, M.H.; Kim, K.S.; Park, J.C. Comparative Study of Standard WC-SPH and MPS solvers for Free Surface Academic Problems. *Int. J. Offshore Pol. Eng.* **2016**, *26*, 235–243. [CrossRef]
27. Kim, K.S.; Kim, M.H.; Park, J.C. Development of moving particle simulation method for multiliquid-layer sloshing. *Math. Probl. Eng.* **2014**, *2014*, 350165. [CrossRef]
28. Kim, K.S. A Mesh-Free Particle Method for Simulation of Mobile-Bed Behavior Induced by Dam Break. *Appl. Sci.* **2018**, *8*, 1070. [CrossRef]
29. Ng, K.C.; Alexiadis, A.; Ng, Y.L. An improved particle method for simulating Fluid-Structure Interactions: The multi-resolution SPH-VCPM approach. *Ocean Eng.* **2022**, *24*, 110779. [CrossRef]
30. Cundall, P.A.; Strack, O.D.L. A discrete numerical model for granular assemblies. *Géotechnique* **1979**, *29*, 47–65. [CrossRef]
31. Spinewine, B. Two-Layer Flow Behaviour and the Effects of Granular Dilatancy in Dam-Break Induced Sheet-Flow. Ph.D. Thesis, University Catholique de Louvain, Ottignies-Louvain-la-Neuve, Belgium, 2005.
32. Kim, K.S. Solid Particle Simulation with a New Particle Interaction. *IEIE Trans. Smart Process. Comput.* **2021**, *10*, 369–374. [CrossRef]
33. Kim, K.S. A Study of Sediment Behavior for Dam-Break Flow over Granular Bed. *Mathematics* **2025**, *13*, 3919. [CrossRef]
34. Wen, C.Y. Mechanics of fluidization. In *Fluid Particle Technology. The Chemical Engineering Progress Symposium Series*; American Institute of Chemical Engineers: New York, NY, USA, 1966; Volume 62, pp. 100–111.


**Disclaimer/Publisher's Note:** The statements, opinions and data contained in all publications are solely those of the individual author(s) and contributor(s) and not of MDPI and/or the editor(s). MDPI and/or the editor(s) disclaim responsibility for any injury to people or property resulting from any ideas, methods, instructions or products referred to in the content.